DOI: 10.1002/ejic.200600274

Chemical and Electrochemical Behaviours of a New Phenolato-Bridged Complex $[(L)Mn^{II}Mn^{II}(L)]^{2+}$. Pathways to Mononuclear Chlorido $[(L)Mn^{II/III/IV}Cl]^{0/1/2+}$ and Dinuclear Mono-μ-Oxido $[(L)Mn^{III}(\mu\text{-}O)Mn^{III/IV}(L)]^{2+/3+}$ Species

Laurent Sabater,[a] Christelle Hureau,*[a,b] Guillaume Blain,[a] Régis Guillot,[a] Pierre Thuéry,[c] Eric Rivière,[a] and Ally Aukauloo*[a]

Keywords: Manganese / N,O Ligands / Chloride ions / Electrochemistry / EPR spectroscopy

The X-ray structure of a new dinuclear phenolato-bridged Mn_2^{II} complex abbreviated as $[(L)MnMn(L)]^{2+}$ (**1**), where LH is the $[N_4O]$ phenol containing ligand *N*,*N*-bis(2-pyridylmethyl)-*N*′-salicylidene-ethane-1,2-diamine ligand, is reported. A *J* value of –3.3 cm^{-1} ($H = -J\hat{S}_1\cdot\hat{S}_2$) was determined from the magnetic measurements and the 9.4 GHz EPR spectra of both powder and frozen acetonitrile solution samples were analyzed with temperature. The cyclic voltammetry of **1** displays a reversible anodic wave at $E^{1/2}$ = 0.46 V vs. SCE associated with the two-electron oxidation of **1** yielding the dinuclear Mn_2^{III} complex $[(L)MnMn(L)]^{4+}$ (**2**). The easy air oxidation of **1** gives the mono-μ-oxido Mn_2^{III} complex $[(L)Mn(\mu\text{-}O)Mn(L)]^{2+}$ (**3**). A rational route to the formation of the mixed-valence $Mn_2^{III,IV}$ complex $[(L)Mn(\mu\text{-}O)Mn(L)]^{3+}$ (**4**) starting from **1** by bulk electrolysis at E^{p} = 0.75 V vs. SCE in the presence of one equiv. of base per manganese ion is also briefly reported. Addition of chloride ions to **1** led to the cleavage of the phenolato bridges to give the mononuclear Mn^{II} complex [(L)MnCl] (**5**). Cyclic voltammetry of **5** displays two reversible anodic waves at $E^{1/2}$ = 0.21 and $E^{1/2}$ = 1.15 V vs. SCE, assigned to the two successive one-electron abstractions giving the Mn^{III} and Mn^{IV} species $[(L)MnCl]^{+}$ (**6**) and $[(L)MnCl]^{2+}$ (**7**), respectively. The electronic signatures from UV/Visible and EPR spectroscopy of the electrochemically prepared samples of **6** and **7** confirmed the respective oxidation states. For instance, **7** displays a broad and intense absorption band characteristic of a phenolato to Mn^{IV} charge-transfer transition at 690 nm (2000 $M^{-1}cm^{-1}$) and its 9.4 GHz EPR spectrum shows a strong transition at g = 5.2 consistent with a rhombically distorted S = 3/2 system with a zero-field splitting dominating the Zeeman effect.

Introduction

Manganese ions are involved in the structure and activity of numerous metalloenzymes.[1,2] Their nuclearities may vary from 1 to 4 metal ions and they often carry out multielectron redox reactions. A mononuclear Mn core is encountered in superoxide dismutase[3–5] and in oxalate oxidase[6,7] and oxalate decarboxylase,[6,8] while dinuclear centres are the most common[9] and are found in catalase,[3,9,10] arginase,[11,12] and ribonucleotide reductase.[13] A tetranuclear Mn core is the heart of the oxygen-evolving complex of photosystem II.[14,15] The fact that these manganese containing enzymes perform crucial reactions in different processes for the maintenance of terrestrial life has encouraged the chemists to pay particular attention to their functioning mode together with their intimate structures and spectroscopic characterizations. Furthermore, bioinorganic chemists have set the challenge to devise synthetic low molecular weight models[16–18] to either reproduce the coordination spheres of these Mn containing active sites or even more challenging, to mimic the activity of the target enzyme (see for examples ref.[19–23]).

Results on both bases have until now been encouraging but a great effort is still needed to reach our objectives. Research along this field is being pursued in our laboratory. Recently, we have reported on the metalation of the ligand LH, where LH is the $[N_4O]$ phenol-containing ligand *N*,*N*-bis(2-pyridylmethyl)-*N*′-salicylidene-ethane-1,2-diamine, with Mn^{II} salt giving the $[(LH)MnCl_2]$ complex where the phenol was still in a protonated state.[24] We have shown through various spectroscopic characterizations that upon the first one-electron oxidation process a concerted chemical reaction took place with the concomitant expulsion of one chloride ion from the manganese coordination sphere together with the deprotonation of the phenol and the coor-

[a] Institut de Chimie Moléculaire et des Matériaux d'Orsay, UMR 8182, Université Paris-Sud,
91405 Orsay Cedex, France
E-Mail: christelle.hureau@cea.fr; aukauloo@icmo.u-psud.fr
[b] Current address: Département de Biologie Joliot-Curie, Service de Bioénergétique, URA 2096, CEA Saclay,
91191 Gif-sur-Yvette Cedex, France
[c] CEA Saclay, DRECAM/SCM,
Bâtiment 125, 91191 Gif-sur-Yvette, France

Supporting information for this article is available on the WWW under http://www.eurjic.org or from the author.

dination of the phenolate group. The reversibility of this process was also evidenced. We believe that such an electrochemical process is essential to delineate the highly intricate manganese chemistry. Herein we report on the synthesis of the dinuclear phenolato-bridged Mn_2^{II} species $[(L)Mn\text{-}Mn(L)]^{2+}$ (**1**), which has been characterized by X-ray diffraction studies, EPR spectroscopy, and cyclic voltammetry. We show that complex **1** can withstand a two-electron oxidation leading to complex $[(L)MnMn(L)]^{4+}$ (**2**) keeping the phenolate groups as bridging ligands. However, upon air oxidation of **1**, the mono-μ-oxido-bridged Mn_2^{III} complex $[(L)Mn(\mu\text{-}O)Mn(L)]^{2+}$ (**3**) is obtained while the corresponding mixed-valence $Mn_2^{III,IV}$ complex $[(L)Mn(\mu\text{-}O)\text{-}Mn(L)]^{3+}$ (**4**) is electrochemically generated. A more detailed study on the reaction of complex **1** with the biologically ubiquitous chloride ions is described. After addition of chloride ions the mononuclear Mn^{II} species [(L)MnCl] (**5**) is formed. The electrochemical behaviour of **5** exhibits two one-electron reversible-oxidation processes, changing the initial Mn^{II} to Mn^{III} and Mn^{IV} oxidation states, respectively. Spectroscopic characterizations of the Mn^{III} $[(L)\text{-}MnCl]^{+}$ (**6**) and Mn^{IV} $[(L)MnCl]^{2+}$ (**7**) complexes in the $[N_4OCl]$ environment are reported.

Results

Characterization of Complex $[(L)MnMn(L)]^{2+}$ (1)

The reaction of ligand LH with $Mn(ClO_4)_2{\cdot}6H_2O$ in ethanol, and in the presence of one equiv. of 2,6-dimethylpyridine gives the complex $\mathbf{1}(ClO_4)_2{\cdot}2H_2O$. In order to attenuate the extremely fast air oxidation of **1** into the mono-μ-oxido-bridged Mn_2^{III} complex $[(L)Mn(\mu\text{-}O)Mn(L)]^{2+}$ (**3**) (see Exp. Sect. for details), the preparation and handling of complex **1**, except for the magnetic measurements, were performed under an argon flux. Nevertheless, unavoidable contamination of solution and solid samples of complex **1** by complex **3** were observed by cyclic voltammetry and by UV/Visible spectroscopy.

X-ray Crystal Structure of $\mathbf{1}(ClO_4)_2{\cdot}2CH_3CN$

The X-ray structure of complex **1** is shown in Figure 1, and principal bond lengths and angles are listed in Table 1. The structure consists of a discrete cation $[(L)Mn\text{-}Mn(L)]^{2+}$ (**1**), two perchlorate anions, and two acetonitrile solvent molecules. The two Mn^{II} centres are bridged by the phenolato groups of the two L^- ligands. Therefore, a $[N_4O_2]$ donor set forms the distorted octahedral coordination environment of each Mn ion. Bond lengths and angles listed in Table 1 show the distortion from octahedral geometry due to constraints imposed by the ligand.

The Mn···Mn distance of 3.383 Å is slightly longer than those reported for phenolato-bridged Mn_2^{II} complexes of closely related mL^-, Li^-/La^- ligands (see Scheme 1),[25–27] but shorter than those obtained for phenolato-bridged Mn_2^{II} complexes obtained with the $[N_3O_2Cl]$ metal environment.[28] As a matter of fact, the Mn_2O_2 diamond core structure of **1** differs from those of complexes $[(mL)Mn\text{-}Mn(mL)]^{2+}$ and $[(Li/La)MnMn(Li)]^{2+}$.[29] Values of the average Mn–O–Mn angle and of the dihedral angle are slightly greater than those observed in $[(mL)Mn\text{-}Mn(mL)]^{2+}$ and $[(Li/La)MnMn(Li)]^{2+}$ systems: 103.7° vs. 100.0° and 101.4°, and 17.9° vs. 11.3° and 11.5°, respectively.[26,27] This can be tentatively attributed to the conjugation of the bridging phenolato group to an imine function in the present case.

The wrapping of the Mn ion by the ligand L^- is identical to that observed in the structures of related Mn[24,30] and Fe[31] complexes, with the two pyridine functions in a *trans* position to one another.

Magnetic Susceptibility Measurements

The molar magnetic susceptibility χ_M of a powder sample of $\mathbf{1}(ClO_4)_2{\cdot}2H_2O$ was measured between 300 and 2 K. At 300 K the $\chi_M T$ value is equal to 6.8 $cm^3\,mol^{-1}\,K$ and decreases slowly down to 5.0 $cm^3\,mol^{-1}\,K$ at 50 K. Below 50 K the $\chi_M T$ value decreases more rapidly and is equal to 0.3 $cm^3\,mol^{-1}\,K$ at 2 K (Figure S1, open circles). This behaviour is indicative of a weak antiferromagnetic interaction between two high-spin Mn^{II} ions ($S = 5/2$). The best simulation performed on the χ_M vs. T curve is obtained with a fixed g value of 1.95[32] and $J = -3.2\ cm^{-1}$ ($H = -J\hat{S}_1{\cdot}\hat{S}_2$) (Figure S1, solid line).[33] The best simulation performed on the $\chi_M T$ vs. T curve is obtained with $g = 1.95$[32] and $J = -3.4\ cm^{-1}$ (Figure S1, solid line).[34] The two sets of parameters are in agreement and lead to a J value that is close to $-3.3(0.1)\ cm^{-1}$. This value is consistent with reported J values for systems where the two Mn^{II} ions are bridged by two phenolato groups,[35–38] and is slightly higher than the one published for the closely related $[(mL)MnMn(mL)]^{2+}$ complex.[27]

EPR Spectroscopy

The 9.4 GHz (X band) EPR spectra recorded at 5 and 30 K, and the 10 K 34 GHz (Q-band) EPR spectrum of a powder sample of $\mathbf{1}(ClO_4)_2{\cdot}2H_2O$ are shown in Figure 2(a,b). The evolution of the 9.4 GHz EPR signatures as a function of temperature was monitored between 5 and 50 K and is given in the Supporting Information (Figure S2). All spectra exhibit features extending from 0–800 mT at 9.4 GHz and from 400–1500 mT at 34 GHz, the intensities of which depend on the temperature. This behaviour is strongly indicative of dinuclear Mn_2^{II} species.[35,38–42] The observed features originate from the superimposition of signatures from the five $S = 1$ to $S = 5$ paramagnetic spin states.[43] The 9.4 and 34 GHz EPR spectra that were

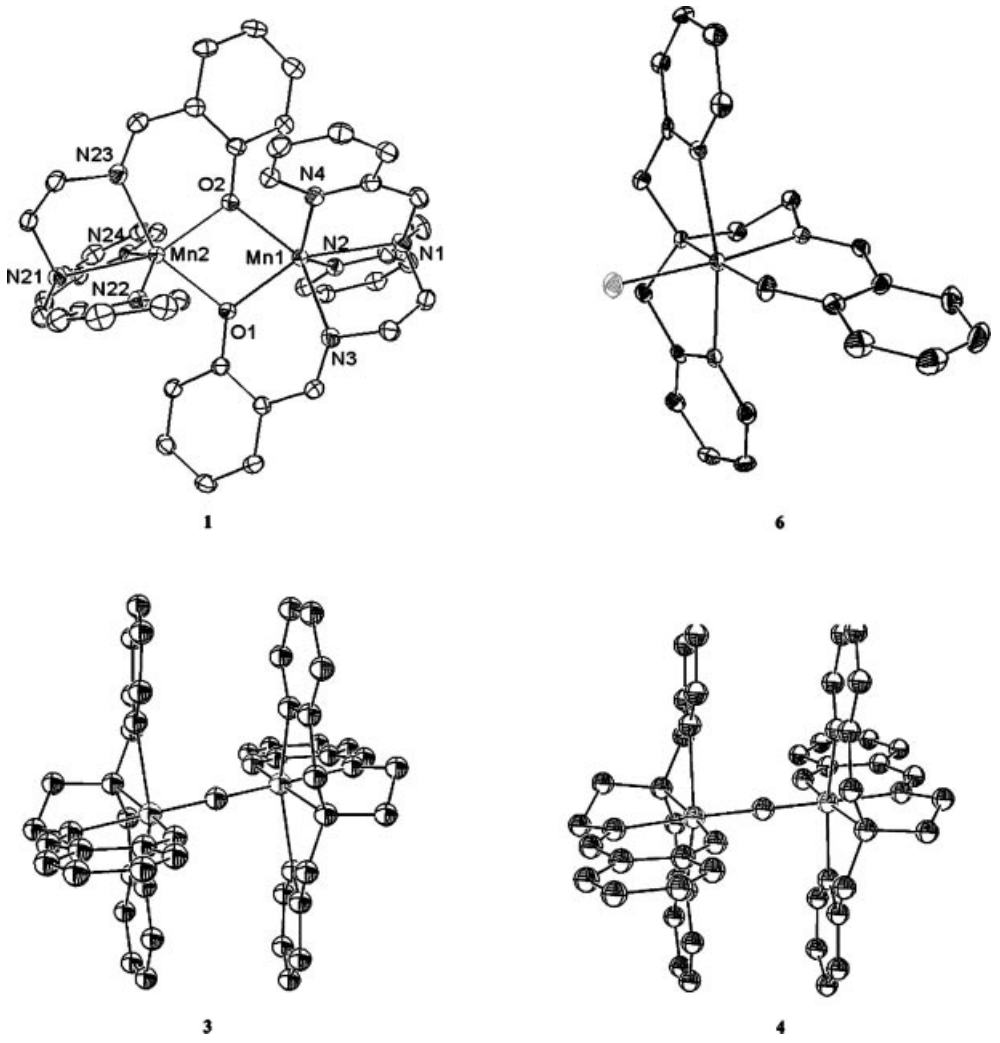

Figure 1. Molecular view of the dication **1**. Displacement ellipsoids are drawn at the 50% probability level. Molecular views of cations **3**, **4**, and **6** from ref.[24,30].

Table 1. Selected bond lengths [Å] and angles [°] for **1**.

Mn1–O1	2.166(2)	Mn2–O1	2.137(2)
Mn1–O2	2.154(2)	Mn2–O2	2.144(2)
Mn1–N1	2.406(2)	Mn2–N21	2.373(3)
Mn1–N2	2.222(3)	Mn2–N22	2.274(3)
Mn1–N3	2.204(3)	Mn2–N23	2.196(3)
Mn1–N4	2.290(3)	Mn2–N24	2.241(3)
O1–Mn1–O2	73.10(8)	O1–Mn2–O2	73.89(10)
Mn1–O1–Mn2	103.68(10)	Mn1–O2–Mn2	103.84(10)
O1–Mn1–N1	151.69(10)	O2–Mn2–N21	156.94(10)
O2–Mn1–N1	133.31(10)	O1–Mn2–N21	128.61(10)
O1–Mn1–N2	94.95(10)	O2–Mn2–N22	118.41(10)
O2–Mn1–N2	99.90(12)	O1–Mn2–N22	84.26(10)
O1–Mn1–N3	80.95(10)	O2–Mn2–N23	82.13(10)
O2–Mn1–N3	147.47(10)	O1–Mn2–N23	149.03(10)
O1–Mn1–N4	126.60(10)	O2–Mn2–N24	100.16(10)
O2–Mn1–N4	84.48(10)	O1–Mn2–N24	101.97(10)
N1–Mn1–N2	72.90(10)	N21–Mn2–N22	73.83(10)
N1–Mn1–N3	76.81(10)	N21–Mn2–N23	78.15(10)
N1–Mn1–N4	73.47(10)	N21–Mn2–N24	72.43(10)
N2–Mn1–N3	101.58(12)	N22–Mn2–N23	90.39(12)
N2–Mn1–N4	137.04(10)	N22–Mn2–N24	140.96(10)
N3–Mn1–N4	95.94(12)	N23–Mn2–N24	101.29(12)

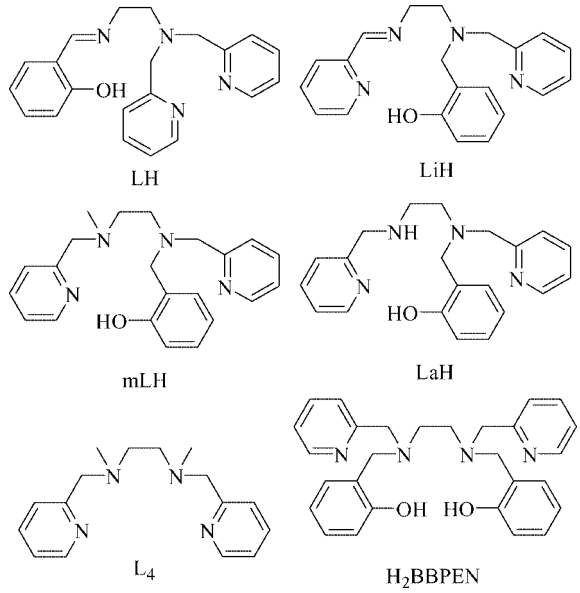

Scheme 1. The LH ligand used in this work and related ligands for comparison.

obtained are slightly different from those previously reported for the $[(mL)MnMn(mL)]^{2+}$ complex.[27] More precisely, the 34 GHz EPR spectrum of the $[(mL)MnMn(mL)]^{2+}$ complex shows several lines below 600 mT, which are attributed to inter-S-spin transitions from the competitive effect between the Zeeman and the Heisenberg interactions ($J = -1.8\ cm^{-1}$).[27] Here, the 34 GHz EPR spectrum of **1** shows only one transition below 600 mT, in agreement with the higher J value of $-3.3\ cm^{-1}$.

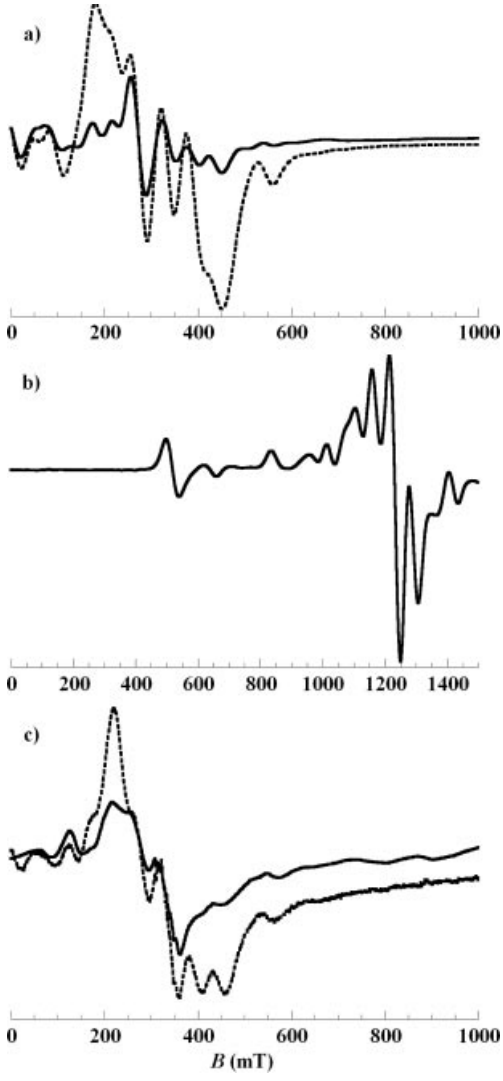

Figure 2. (a) 9.4 GHz EPR spectra recorded on a powder sample of $\mathbf{1}(ClO_4)_2{\cdot}2H_2O$ at 5 K (solid line) and 30 K (dotted line). (b) 34 GHz EPR spectra recorded on a powder sample of $\mathbf{1}(ClO_4)_2{\cdot}2H_2O$ at 10 K. (c) 9.4 GHz EPR spectra recorded on a millimolar solution sample of **1** in acetonitrile containing 0.1 M tetrabutylammonium perchlorate at 5 K (solid line) and 30 K (dotted line). Note that the product of the absorption by the temperature T is plotted as a function of the magnetic field. 9.4 GHz EPR recording conditions: 9.38 GHz microwave frequency, 2.0 mW microwave power, 0.5 mT modulation amplitude, 100 kHz modulation frequency. 34 GHz EPR recording conditions: 34.18 GHz microwave frequency, 2.3 mW microwave power, 1.0 mT modulation amplitude, 100 kHz modulation frequency.

The 9.4 GHz EPR spectra recorded at 5 and 30 K of a frozen acetonitrile solution sample of **1** in the presence of 0.1 M tetrabutylammonium perchlorate are shown in Figure 2 (c). Evolution of the 9.4 GHz EPR signatures as a function of temperature is given in the Supporting Information (Figure S3). The EPR signatures as well as the modifications in the relative intensities of the observed EPR features as a function of temperature conform to that of a dinuclear Mn_2^{II} species. The evolution of the EPR features is similar to the one observed in the powder sample of complex **1**. More precisely, in both powder and solution samples, the features near 200 and 400 mT increase with the temperature. Therefore, we can rationally propose that the dinuclear phenolato-bridged Mn_2^{II} core structure is maintained upon dissolution in acetonitrile. However, no characteristic ^{55}Mn hyperfine pattern is observed. This can be attributed either to the superimposition in the same magnetic field range of several lines originating from different transitions that exhibit slightly distinct Mn hyperfine structures, or to a structural heterogeneity that would induce a distribution in the EPR parameters.

UV/Visible Spectroscopy

The UV/Visible spectrum of complex **1** is shown in Figure 3 (a, dashed line) and the UV/Visible data are reported in Table 2. As expected for Mn^{II} species no transition is observed in the visible region. An intense band is detected at 348 nm, which can be tentatively attributed to the phenolato to Mn^{II} charge-transfer transition by comparison with data obtained from the related $[(L')Mn]^-$ complex, where $L'H_3$ is a triphenol containing ligand with a $[N_2O_3]$ donor set.[25,44] The band detected at 300 nm and indicated by an asterisk in Figure 3 (a) is assigned to the contaminant species **3** (see Table 2).

Cyclic Voltammetry

The cyclic voltammogram of complex **1** is shown in Figure 4 (a) and its redox data are reported in Table 3. Anodic and cathodic processes assigned to the soil species **3** are indicated by a star in Figure 4 (a). The cyclic voltammetry trace of **1** exhibits a reversible anodic process at $E^{1/2} = 0.46$ V vs. SCE ($\Delta E^P = 133$ mV),[45] and an irreversible anodic peak at $E^P = 1.44$ V vs. SCE. The square wave voltammetry shows that two and one electrons are involved in the first and the second anodic process, respectively. These data indicate that the first anodic process is associated with the formation of the dinuclear phenolato-bridged Mn_2^{III} complex $[(L)MnMn(L)]^{4+}$ (**2**), while the second anodic process is associated with the formation of a Mn^{IV} containing species. Irreversibility of the second anodic process is probably due to the generation of a Mn^{IV} ion, which would spontaneously engender the opening of the dinuclear structure. For comparison purposes redox data of complex **1** together with other related dinuclear phenolato-bridged Mn_2^{II} complexes are given in Table 3. The potential value of the first

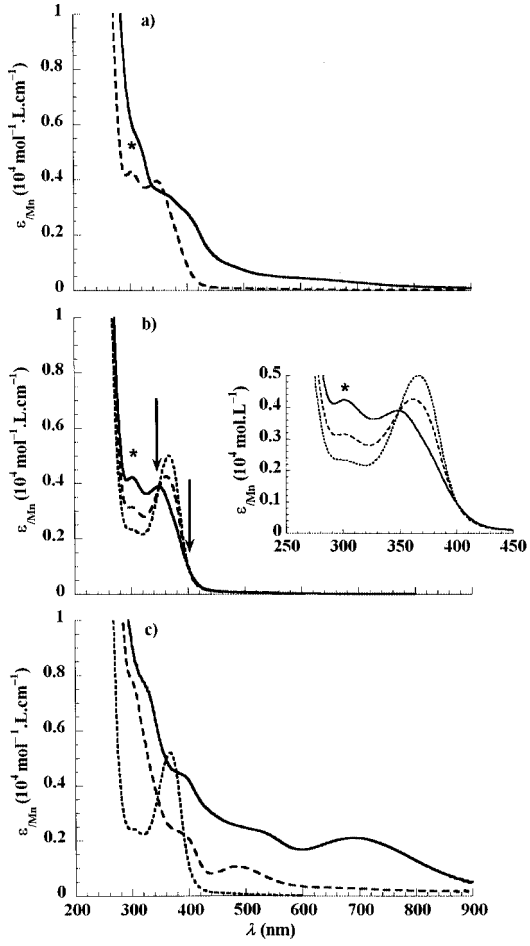

Figure 3. (a) UV/Visible spectrum of complex **1** in acetonitrile containing 0.1 M tetrabutylammonium perchlorate (dashed line) and of complex **2**, generated by exhaustive electrolysis of **1** at E = 0.8 V vs. SCE (solid line); (b) UV/Visible spectrum of 1 mM solution of **1** in acetonitrile containing 0.1 M tetrabutylammonium perchlorate, upon addition of chloride ions. No chloride ion added (solid line), 0.5 equiv. of chloride ion per Mn (dashed line) and 1.0 equiv. of chloride ion per Mn ion (dotted line); (c) UV/Visible spectrum of complex **5**,[60] (dotted line); of complex **6**, generated by exhaustive electrolysis of complex **5** at E = 0.85 V vs. SCE (dashed line), and of complex **7**, generated by exhaustive electrolysis of complex **5** at E = 1.45 V vs. SCE (solid line). (l = 1 mm, T = 20 °C). Note that unless specified the total conversions of **1** were assumed to draw the absorption spectrum. The asterisks * in (a) and (b) indicate the presence of the contaminant species **3**.

anodic process of **1** is lower than those of related phenolato-bridged dinuclear Mn_2^{II} complexes, and the peak-to-peak separation ΔE^P is distinctly smaller. The possible origins of these differences will be discussed below.

An irreversible cathodic peak is detected at E^P = –1.91 V vs. SCE, while in the related $[(Li/La)MnMn(Li)]^{2+}$ complex[29] reduction of the imine function of the Li^- ligand (see Scheme 1) was observed at E^P = –1.38 V vs. SCE.[26] The conjugation of the imine function to a phenolato group in the L^- is anticipated to render the reduction more difficult, and therefore explain the lower potential value detected here.

Electrochemical Oxidation of Species 1 into Complex [(L)MnMn(L)]$^{4+}$ (2)

The square wave and the cyclic voltammetry experiments recorded on complex **1** indicate that oxidation of **1** will lead to the dinuclear phenolato-bridged Mn_2^{III} species $[(L)MnMn(L)]^{4+}$ (**2**). Exhaustive electrolysis was performed at E = 0.8 V vs. SCE. The cyclic voltammetry trace recorded after consumption of one electron per Mn ion displays one reversible cathodic process at $E^{1/2}$ = 0.46 V vs. SCE and one irreversible anodic peak E^P = 1.44 V vs. SCE (Figure S4). These data are consistent with the formation of complex **2** in solution. An insignificant amount of the dinuclear mono-μ-oxido-bridged complexes was generated during the electrolysis.

The UV/Visible spectrum recorded after completion of the electrolysis is shown in Figure 3 (a, solid line), and the UV/Visible data reported in Table 2, together with those of related phenolato Mn^{III} complexes. Upon comparison, it is possible to attribute the broad transition detected near 600 nm to Mn^{III} d–d transitions and the shoulder observed at 480 nm to the superimposition of Mn^{III} d–d transitions and phenolato to Mn^{III} charge-transfer transitions. Both the position and the intensity of the two absorption bands detected near 405 nm agree with values reported in the literature for bridging phenolato to Mn^{III} charge-transfer transitions.[44,46–49] The shift of the phenolato to Mn^{II} electronic transition detected in **1** at 348 nm to a lower energy upon oxidation of the Mn ion is reminiscent of what was observed for the successive oxidations of the dinuclear Mn_2^{II} complex $[Mn_2(2\text{-}OHsalpn)_2]^{2-}$.[25,50] The UV/Visible signature of complex **2** is very close to that of complex **3**, except for the strong absorption band at 300 nm only detected in **3**.

9.4 GHz EPR spectra were recorded on the electrolyzed solution using the perpendicular and the parallel detection modes (data not shown). No signal was detected.

Electrochemical Conversion of Species 1 into Complex [(L)Mn(μ-O)Mn(L)]$^{3+}$ (4)

The electrochemical conversion of mono- and dinuclear Mn^{II} complexes into mixed-valence oxido-bridged $Mn_2^{III,IV}$ systems has been recently described.[27,51,52] An exhaustive electrolysis of the Mn^{II} species is performed in acetonitrile, where the presence of residual water together with an external base leads to the formation of the oxido-bridged species. This method was applied here to obtain the mixed-valence complex $[(L)Mn(\mu\text{-}O)Mn(L)]^{3+}$ (**4**).

The cyclic voltammetry trace of species **1** upon addition of one equiv. of base per Mn ion is shown in Figure 4 (b). When scanning towards anodic potentials, the first oxidation process of species **1** is still partially detected, but at a slightly lower potential value. Furthermore, two new reversible processes are seen at $E^{1/2}$ = 0.55 and $E^{1/2}$ = 1.0 V vs. SCE, which correspond to the two sequential one-electron oxidations of the dinuclear Mn_2^{III} complex $[(L)Mn(\mu\text{-}O)Mn(L)]^{2+}$ (**3**). Both the detection of the oxidation

Table 2. Electronic absorption data of complexes **1** to **7** and of the related complexes $[(L_4)MnCl_2]^+$, $[(L_4)MnCl_2]^{2+}$, $[(BBPEN)Mn]^+$, and $[(BBPEN)Mn]^{2+}$.[25]

Species	λ, $\varepsilon_{/Mn}$ (nm, 10^3 M^{-1}cm^{-1})				Ref.
Mn^{II}					
1	348, 3.9				this work
5	367, 5.0				this work
Mn^{III}					
2	370, 3.4	405, 2.7	480, 0.88	600, 0.47	this work
6	298, 7.5	392, 2.1	479, 0.98	494, 1.01	this work
$[(L_4)MnCl_2]^+$	291, 7.1	394, 1.1	500, 0.30	536, 0.36	[52]
$[(BBPEN)Mn]^+$	258, 29	369, 4.2	506, 2.1		[54]
3	300, 10.5	400, 2.4	500, 0.5		[30]
Mn^{IV}					
7	325, 7.2	390, 4.2	523, 2.2	690, 2.0	this work
$[(L_4)MnCl_2]^{2+}$	314, 8.5	409, 2.2			[52]
$[(BBPEN)Mn]^{2+}$			506, 2.7	790, 3.7	[54]
4	344, 6.2	408, 3.5	570, 1.5		[30]

peak of **1** at a lower potential value and of the cyclic voltammetry signature of a new species are symptomatic of an EC (Electrochemical Chemical) mechanism. Oxidation of species **1** leading to the corresponding dinuclear Mn_2^{III} species **2** is followed by the formation of complex **3** at the electrode, because of the presence of residual water and of base in the medium.[53] This EC mechanism is illustrated in Scheme 2.

The cyclic voltammogram, the UV/Visible spectrum, and the 100 K 9.4 GHz EPR spectrum recorded after bulk electrolysis at 0.75 V vs. SCE (Figure 4(c), Figures S5, and S6, respectively, in the Supporting Information) are identical to those reported for the mixed-valence complex **4** obtained by the one-electron oxidation of the chemically prepared species **3**.[30] Both the number of consumed electrons during the electrolysis (3 e^- per complex **1**) and the extinction coefficient values are consistent with the total conversion of species **1** into **4**. This is confirmed by quantification of the EPR trace recorded after the electrolysis of **1** (Figure S6), which shows the formation of **4** with a 95% (±5%) yield (see Exp. Sect. for details).

Transformation of Complex 1 upon Addition of Chloride Ions

Evolution of the cyclic voltammetry trace of complex **1** upon addition of 0.5 and 1.0 equiv. of chloride ion per Mn ion is shown in Figure 4 (d dashed and solid lines, respectively). The anodic process corresponding to the oxidation of free chloride ions is not observed. Concomitantly with the loss of the anodic processes related to complex **1**, two new reversible anodic processes were detected at $E^{1/2}$ = 0.21 (ΔE^P = 95 mV) and $E^{1/2}$ = 1.15 V vs. SCE (ΔE^P = 94 mV). By comparing the potential values with those of related complexes with $[N_4Cl_2]$[52] and $[N_4O_2]$[54] Mn environments (see Table 3) we propose that the coordination sphere of the Mn ion is $[N_4OCl]$ provided by the L^- ligand and one exogenous chloride anion, leading to the neutral Mn^{II} species [(L)MnCl] (**5**). In this hypothesis, the two anodic processes are attributed to the successive one-electron oxidation of species **5** into the mononuclear Mn^{III} $[(L)MnCl]^+$ (**6**) complex and then into the mononuclear Mn^{IV} $[(L)MnCl]^{2+}$ (**7**) complex.

The spectral changes of the UV/Visible spectrum of complex **1** upon addition of 0.5 and 1.0 equiv. of chloride ion per Mn ion are shown in Figure 3 (b, dashed and dotted lines, respectively). The phenolato to Mn^{II} charge transfer transition detected at 348 nm for complex **1** is shifted to lower energies (λ_{max} = 367 nm) in species **5**. This spectral modification can be related to the change in the coordination mode of the phenolato arm from bridging to monodendate.

By contrast to the modifications observed by cyclic voltammetry and UV/Visible spectroscopy at room temperature, the EPR signature of complex **1** recorded at 100 K is virtually unmodified upon the addition of one equiv. of chloride ion per Mn ion (Figure 5, a,b). It totally vanishes upon the addition of five equiv. of chloride ions per Mn ion (Figure 5, d). The new spectral features consist of an intense transition at 330 mT (g = 2) and three other transitions of lower intensity at 50 mT, 130 mT, and 225 mT. This signature is consistent with a mononuclear Mn^{II} species, where the Zeeman effect dominates the zero-field splitting interaction.[55–59] The EPR study gives a first insight into the presence of an equilibrium between species **1**, **5**, and the chloride ions, which should be modified by the temperature. The detection of this equilibrium at room temperature was monitored by cyclic voltammetry. Upon addition of two and five equiv. of chloride ions per Mn ion, the cyclic voltammetry trace shows that the potential of the anodic peak is slightly shifted to lower values, whereas the position of the associated cathodic peak observed on the reverse scan remains virtually identical (Figure S7). This behaviour is reminiscent of a CE (Chemical-Electrochemical) mechanism, which is illustrated in Scheme 3. As a working hypothesis, we propose that the chemical reaction, which precedes the electrochemical oxidation of species **5** into **6**, is an equilibrium between species **1** and **5**.

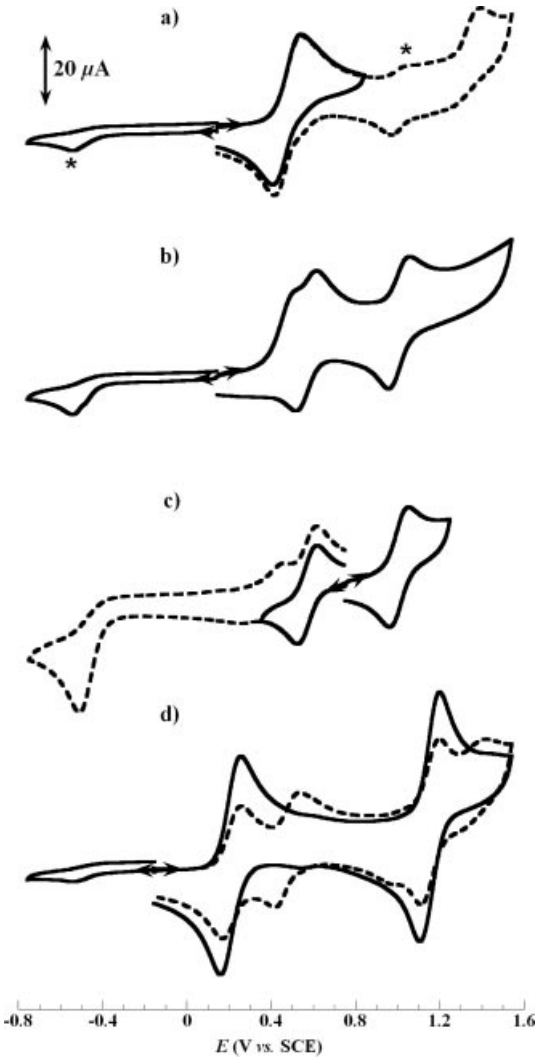

Figure 4. (a) Cyclic voltammograms of 1 mM solution of **1** in acetonitrile containing 0.1 M tetrabutylammonium perchlorate. (b) Cyclic voltammograms of 1 mM solution of **1** in acetonitrile in presence of one equiv. of 2,6-dimethylpyridine per Mn ion. (c) Cyclic voltammograms of 1 mM solution of **1** in acetonitrile in the presence of one equiv. of 2,6-dimethylpyridine per Mn ion, and after bulk electrolysis at E = 0.7 V vs. SCE. (T = 20 °C, scan rate = 100 mV). (d) Cyclic voltammograms of 1 mM solution of **1** in acetonitrile in the presence of 0.5 equiv. of chloride ion per Mn ion (dashed line), and in the presence of 1.0 equiv. of chloride ion per Mn ion (solid line). The stars in (a) indicate the presence of the contaminant species **3**.

It is worth noting that upon the addition of chloride ions, the intensity of anodic and cathodic processes corresponding to the contaminant species **3** fades significantly, as well as the UV band detected at 300 nm and assigned to species **3**. The dissipation of species **3** upon addition of chloride ions will be considered below.

Electrochemical Oxidations of Complex 5 into Species $[(L)MnCl]^+$ (6) and $[(L)MnCl]^{2+}$ (7)

The cyclic voltammetry signature of complex **5**,[60] which is shown in Figure 4(d), suggests that complex **5** can be oxidized twice electrochemically to generate the corresponding Mn^{III} $[(L)MnCl]^+$ (**6**) and Mn^{IV} $[(L)MnCl]^{2+}$ (**7**) species. Two successive bulk electrolysis of species **5** were performed at E = 0.85 (20 °C) and E = 1.45 V vs. SCE (–30 °C), respectively, and were monitored by UV/Visible and EPR spectroscopy.

The cyclic voltammetry trace recorded after the first consumption of one electron per Mn ion displays one reversible anodic process at $E^{1/2}$ = 1.15 V vs. SCE and one reversible cathodic process at $E^{1/2}$ = 0.21 V vs. SCE (Figure S8, dashed line). These data are consistent with the one-electron oxidation of species **5** leading to the mononuclear Mn^{III} complex **6**.

The UV/Visible spectrum recorded after the first bulk electrolysis is shown in Figure 3 (c, dashed line). Three new transitions are detected in the region from 390 to 495 nm. The UV/Visible data of complex **6** are reported in Table 2, together with other related phenolato and chlorido Mn^{III} complexes. Upon comparison, it is possible to attribute the 390 nm absorption band to the superimposition of chlorido and phenolato to Mn^{III} charge-transfer transitions, and the two transitions detected at 479 and 494 nm to both Mn^{III} d–d transitions and phenolato to Mn^{III} charge-transfer transitions.

No EPR signal was detected using the conventional perpendicular detection mode. However, the 5 K 9.4 GHz EPR spectrum of the electrolyzed solution, recorded in the parallel detection mode displays six ill-resolved hyperfine lines centred at 79 mT (g = 8.5) and spaced by 5.4 mT (Figure 6, a). As previously described in the literature, 9.4 GHz parallel mode EPR spectra are expected for an S = 2 quasi-axial system with a strong zero-field splitting.[61,62] More specifically, the spectroscopic signatures detected here are characteristic of a high-spin Mn^{III} species, where the Jahn–Teller distortion is an elongation.[52,63–69]

The cyclic voltammetry trace recorded after the second one-electron electrolysis of **5** displays two reversible cathodic processes at $E^{1/2}$ = 1.15 and $E^{1/2}$ = 0.21 V vs. SCE (Figure S8, solid line), underlying that the one-electron oxidation of species **6** into the mononuclear Mn^{IV} complex **7** was successful. However, a slightly weaker intensity is observed for the two electrochemical processes, indicating a partial evolution of the Mn^{IV} species, even at –30 °C. It is worth noting that the possibility of a ligand-centred oxidation of species **6** leading to the mononuclear Mn^{III}-phenoxyl complex was given some thought. However, it was considered to be an unlikely hypothesis[70] on the basis of the reported oxidation of the Mn^{III} centre at a potential that was 1 V lower than the phenolate ligand in the Mn^{III} species with a phenolate-containing ligand.[71]

The electronic absorption spectrum recorded after the second bulk electrolysis is shown in Figure 3 (c, solid line). Three new intense absorption bands appear at 390, 523, and 690 nm, respectively. The UV/Visible data of complex **7** are reported in Table 3,[72] and compared with related phenolato and chlorido Mn^{IV} complexes. The intense absorption band observed near 400 nm can be attributed to phenolato and chlorido to Mn^{IV} charge-transfer transi-

Table 3. $E^{1/2}$ and E^{p} (when the anodic process is irreversible) potential values (V vs. SCE) of complexes **1** and the related complexes $[(mL)MnMn(mL)]^{2+}$ and $[(Li/La)MnMn(Li)]^{2+}$, of complex **5** and the related complexes $[(L_4)MnCl_2]$ and $[(BBPEN)Mn]^{+}$, and of complex **3**.[25] (T = 20 °C).

Species	E (V vs. SCE), [ΔE^{p} (mV)]		Ref.
	Mn_2^{II}/Mn_2^{III}	$Mn_2^{III}/Mn_2^{III,IV}$	
1	0.46 (133)	1.42 (irr.)[a]	this work
$[(mL)MnMn(mL)]^{2+}$	0.89, 1.02[b]		[27]
$[(Li/La)MnMn(Li)]^{2+}$	0.58 (260)		[26]
	Mn^{II}/Mn^{III}	Mn^{III}/Mn^{IV}	
5	0.21 (96)	1.15 (93)	this work
$[(L_4)MnCl_2]$	0.74 (70)	1.46 (irr.)[a]	[52]
$[(BBPEN)Mn]^{+}$	–0.06 (90)	0.80 (90)	[54]
	$Mn_2^{III}/Mn_2^{III,IV}$	$Mn_2^{III,IV}/Mn_2^{IV}$	
3	0.55 (92)	1.0 (91)	this work[30]

[a] irr. = irreversible. [b] The two potential values correspond to the sequential one-electron oxidation of the Mn_2^{II} complex leading to the Mn_2^{III} complex.

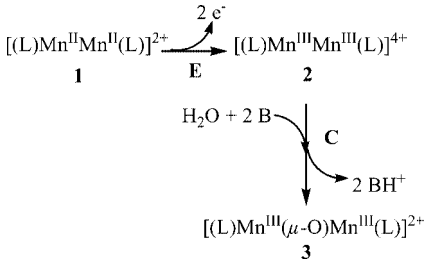

Scheme 2. Proposed Electrochemical Chemical (EC) mechanism to explain the evolution of the cyclic voltammetry trace of **1** upon addition of base.

tions,[71,73] while the shoulder detected at 530 nm may be assigned to Mn^{IV} d–d transitions.[74] However, both the intensity and the position of the broad absorption band observed near 690 nm are reminiscent of absorption features reported for phenolato-containing Mn^{IV} complexes,[27,30,54,71,75–79] and is therefore attributed to a phenolato to Mn^{IV} charge-transfer transition. Therefore, the UV/Vis signature of species **7** also strongly supports the formation of a Mn^{IV} complex instead of a Mn^{III}-phenoxyl one. Indeed, in the latter case, the two observed bands at 400 and 690 nm are expected with stronger and much weaker intensities, respectively.[71]

The 5 K 9.4 GHz EPR spectrum of the electrolyzed solution recorded using the perpendicular detection mode is shown in Figure 6 (b). The EPR spectrum exhibits a multiline signal centred at g = 2 due to the presence of traces of uncoordinated Mn^{II} ions. Quantification of this signal (see Exp. Sect.) indicates that uncoordinated Mn^{II} ions account for approximately 5% of the total Mn-based species. Three other broad transitions are detected at 130 mT (g = 5.2), 220 mT (g = 3.0), and 580 mT (g = 1.2), showing no evidence of ^{55}Mn hyperfine coupling (Figure 6, b). This EPR signature is indicative of an S = 3/2 Mn^{IV} ion, where the zero-field splitting interaction dominates the Zeeman effect.[54,79–86] For an axial Mn^{IV} system (E/D = 0) the low-field transition is expected at g_{eff} = 4. The diver-

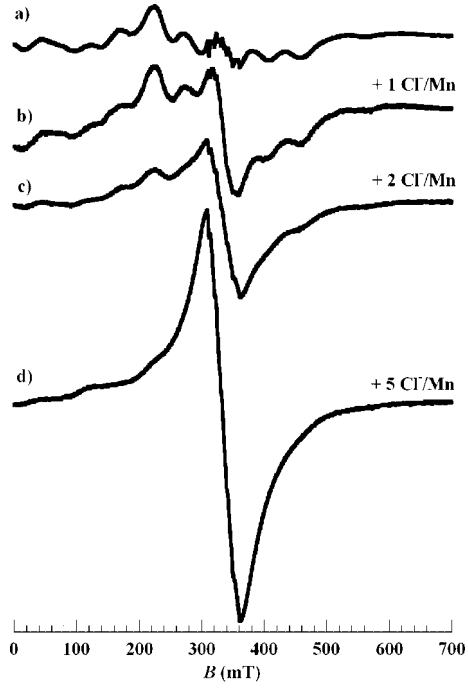

Figure 5. Evolution of the 100 K, 9.4 GHz EPR spectrum of 1 mM solution of **1** in acetonitrile containing 0.1 M tetrabutylammonium perchlorate, upon addition of chloride ions. Recording conditions: 9.38 GHz microwave frequency, 2.0 mW microwave power, 0.5 mT modulation amplitude, 100 kHz modulation frequency.

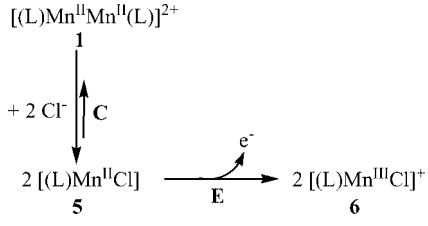

Scheme 3. Proposed Chemical Electrochemical (CE) mechanism to explain the evolution of the cyclic voltammetry trace of **1** upon addition of chloride ions.

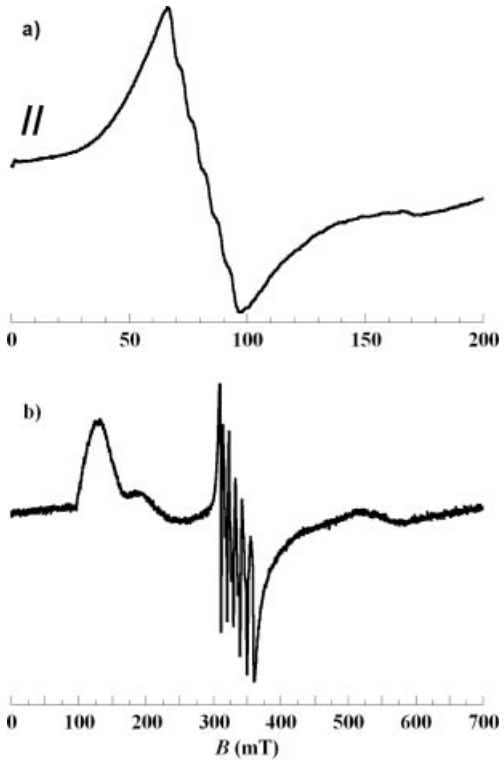

Figure 6. 5 K 9.4 GHz EPR spectra recorded on a 2 mM solution sample of **5**,[60] in acetonitrile containing 0.1 M tetrabutylammonium perchlorate, after bulk electrolysis at E = 0.85 V vs. SCE (a), and after bulk electrolysis at E = 1.45 V vs. SCE (b). Recording conditions: (a) parallel detection mode, 9.42 GHz microwave frequency, 0.8 mW microwave power, 0.5 mT modulation amplitude, 100 kHz modulation frequency, 10 scans. (b) 9.38 GHz microwave frequency, 0.12 mW microwave power, 0.5 mT modulation amplitude, 100 kHz modulation frequency.

gence from this value is characteristic of the rhombicity of the system. In the present case, according to the diagram showing the evolution of the g_{eff} values for the Kramer doublets as a function of E/D,[87] the g_{eff} = 5.2 and g_{eff} = 3.0 values lead to an E/D ratio of 0.20(±0.04).

Discussion

In the first part of this discussion, we will demonstrate the unique physicochemical properties of the dinuclear phenolato-bridged Mn_2^{II} complex (**1**). As it is not our intention here to make an exhaustive comparison among all dinuclear phenolato-bridged Mn_2^{II} complexes,[26,28] we will limit the comparative study to the recently published [(mL)Mn-Mn(mL)]$^{2+}$ system where the Mn ions have almost the same first coordination spheres as in **1**.[27]

Two main structural differences are observed between complex **1** and complex [(mL)MnMn(mL)]$^{2+}$. In the present case, the two pyridine rings are in a *trans* position, and the nitrogen atoms holding the bridging phenolato groups belong to the plane of the Mn_2O_2 core.

These structural peculiarities may support the distinct behaviour found for **1** in solution. More precisely, the enhanced reversibility of the anodic process detected for **1** is assigned to both an easier and nondestructive structural rearrangement from the dinuclear Mn_2^{II} to the dinuclear Mn_2^{III} systems. In the case of complex [(mL)Mn-Mn(mL)]$^{2+}$, it has been proposed that the two successive one-electron oxidations of the dinuclear Mn_2^{II} complex led to the formation of the mononuclear Mn^{III} species.[27] Here, we have shown that the dinuclear structure of complex **1** is maintained upon oxidation. Therefore, we can postulate that the Jahn–Teller distortion axis of the Mn_2^{III} species is along the Py–Mn–Py axis, a direction that is not involved in the bridging motif. Furthermore, oxidation of **1** into **2** is detected at lower potential values than those of the related dinuclear Mn_2^{II} phenolato-bridged complexes (see Table 3). The main difference in the [N_4O] donor set of the ligand L^- compared to the one of ligand mL^- (see Scheme 1) is the conjugation of the phenolate group to an imine function. This is in good agreement with the fact that the imine-phenolate fragment stabilizes the high oxidation states of the metal centres.

A two-electron oxidation process was detected for **1** whereas two successive one-electron oxidations were reported for the [(mL)MnMn(mL)]$^{2+}$ complex. The detection of a two-electron oxidation process is in line with what was observed and analyzed by Romero et al.[42] for the Mn_2^{II} complex [$Mn_2(\mu\text{-}Cl)_2(bpea)_2Cl_2$] where bpea is a tetradentate ligand with a [N_4] donor set.[25] It was interpreted as arising from the independency of the two Mn ions because of a strong insulating effect of the bridging chloride ions. Indeed the two metal centres in the [$Mn_2(\mu\text{-}Cl)_2(bpea)_2Cl_2$] complex must be electronically uncoupled in order not to bring about any stabilization of the mixed-valence state. In the present case, we favour the hypothesis of an inversion of the potentials of the first- and second-electron transfers during the oxidation of **1**, i.e. the oxidation of the mixed-valence $Mn_2^{II,III}$ complex occurs at a lower potential value than that of complex **1**. Hapiot et al. have illustrated the inversion potential phenomenon in polyconjugated systems. Oxidation of the polyconjugated system leads to the dication, which is stabilized by interaction with the solvent, whereas the radical cation, which is delocalized over the molecular framework and thus less stabilized by interactions with the solvent, is not isolated.[88] We thus propose that in our case the easier oxidation of the mixed-valence $Mn_2^{II,III}$ state than that of the Mn_2^{II} state arises from the better stabilization by the solvent of the Mn_2^{III} state than that of the mixed-valence $Mn_2^{II,III}$ system.

Another clear cut difference is the cyclic voltammetry response upon addition of base to a solution of **1** or a solution of the [(mL)MnMn(mL)]$^{2+}$. In the former case, the dinuclear oxido-bridged species **3** is formed on the time scale of the cyclic voltammetry, whereas the intermediate mononuclear Mn^{III} [(mL)Mn(OH)]$^+$ species was proposed in the latter case.[27] This result clearly indicates that the formation of species **3** is faster than that formed in the corresponding Mn^{III} complex [(mL)Mn(μ-O)Mn(mL)]$^{2+}$.

In the second part of the discussion we will examine the various chemical and electrochemical reactions involved be-

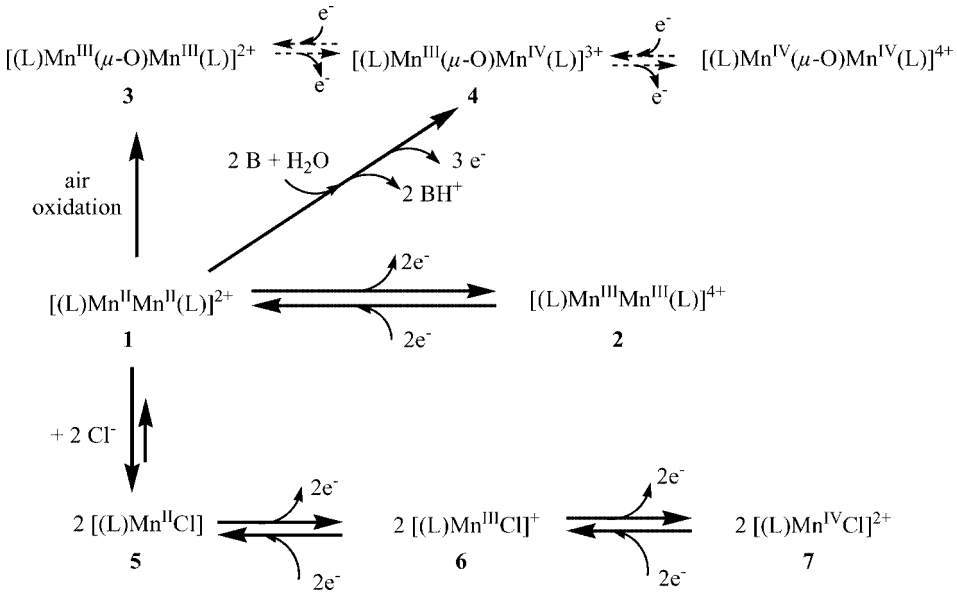

Scheme 4. Scheme of the various chemical or electrochemical reactions involved between species **1** to **7**. Solid arrows correspond to the reactions evidenced in the present work. Dashed arrows correspond to electrochemical processes described in a previous paper.[30]

tween the various Mn species obtained with the ligand L^-, which are depicted in Scheme 4. The X-ray structures of complexes **1**, **3**, **4**, and **6** are available in the present study and in the literature.[24,30]

The presence of the contaminant complex **3** in solution and powder samples of complex **1** has been evidenced by various techniques and comes from the air oxidation of **1**. Since all the experiments are not run in a glove box this impurity is hardly avoidable. The mechanism of this air oxidation is still unknown. The fast air oxidation of **1** may be related to the fast electrochemical oxidation of **1** into **3** in the presence of base as evidenced by the cyclic voltammetry study. We have also shown that the phenolato-bridged dinuclear Mn_2^{III} complex **2** is accessible after a two-electron oxidation of **1** and that it does not evolve directly to the formation of the mono-μ-oxido complex **3** under an argon flux. Such an intermediate will certainly provide hints for the mechanistic pathway of the formation of the mono-μ-oxido species.

We have also checked that the mixed-valence mono-μ-oxido complex **4** can be generated by the exhaustive electrolysis of complex **1** in the presence of residual water and one equiv. of base per Mn ion, following a recently described procedure.[27]

The addition of chloride ions to complex **1** leads to the formation of the mononuclear chlorido Mn^{II} species **5**. One more intriguing result is that upon addition of chloride ions to a solution sample of **1** containing species **3** as an impurity (indicated by an asterisk in parts a,b of Figure 3 and part a of Figure 4) leads to the fading of the absorption transition and of the redox waves characteristic of the mono-μ-oxido species. Furthermore, no other signal except that of species **3** was detected. For now, we can only speculate that species **5** is able to reduce species **3**, leading to the breaking of the oxido bridge by a mechanism that has still to be determined.

More importantly, we have shown that complex **5** can be oxidized twice electrochemically into the corresponding Mn^{III} (**6**) and Mn^{IV} (**7**) complexes. To the best of our knowledge no other (X-ray characterized) mononuclear complexes with a $[N_4OCl]$ coordination sphere are reported in the literature. The spectroscopic data for a Mn^{IV} ion in an unusual coordination sphere with four nitrogen atoms, one oxygen, and a chloride ion are reported.[70] Hence, complex **5** is an interesting example of manganese mononuclear systems where three distinct oxidation states are observed and characterized.

Conclusion

We have shown in this paper the chemical and electrochemical reactivities of a dinuclear phenolato-bridged Mn_2^{II} complex. We have shown that the dinuclear Mn_2^{II} compound could be oxidized in the +III states without alteration of the dinuclear structure of the starting compound. However, addition of chloride ions led to the formation of mononuclear species, which were oxidized and characterized in the +III and the rare +IV oxidation states. Future work will consist of the elucidation of the mechanistic pathways involving the formation of the mono-μ-oxido Mn_2^{III} dinuclear complex.

Experimental Section

General Remarks: Reagents and solvents were purchased commercially and used as received except for the electrochemical experiments for which acetonitrile was distilled under argon over granular $CaCl_2$. Argon U was used in the various experiments.

Caution: Perchlorate salts of metal complexes with organic ligands are potentially explosive. Only small quantities of these compounds should be prepared and handled behind suitable protective shields.

Synthesis

***N*,*N*-Bis(2-pyridylmethyl)-*N'*-salicylidene-ethane-1,2-diamine:** Salicyladehyde (210 μL, 2 mmol) was added to a solution of *N*,*N*-bis(2-pyridylmethyl)ethane-1,2-diamine[89] (484 mg, 2 mmol) in methanol (20 mL). The solution was stirred at room temp for 3 h, evaporated, and dried under vacuum to give a pale brown oil (98% yield). ^{1}H NMR (250 MHz, $CDCl_3$): δ = 8.48 (d, 2 H, J = 5 Hz, *H*–C_6H_3N), 8.24 (s, 1 H, Ar–C*H*=N), 7.60–6.80 (m, 10 H, *H*–Ar), 3.88 [s, 4 H, N–(C*H*$_2$–Py)$_2$], 3.70 (t, 2 H, J = 6 Hz, CH=N–C*H*$_2$–CH_2), 3.46 (s, 1 H, O*H*), 2.90 (t, 2 H, J = 6 Hz, CH_2–*N*–C*H*$_2$–CH_2) ppm; ^{1}H NMR details are given in the Supporting Information. IR: $\tilde{\nu}$ = 3360 (broad), 2944 (strong), 2832 (s), 1634 (medium), 1596 (weak), 1450 (m), 1280 (w), 1028 (s), 762 (w), 660 (br) cm^{-1}. ESI-MS: m/z (%) = 347.2 (100) $[M + H]^+$.

[(L)MnMn(L)](ClO$_4$)$_2$·2(H$_2$O): Ligand LH (173 mg, 0.5 mmol) and 2,6-dimethylpyridine (58 μL, 0.5 mmol) were mixed in air-free absolute ethanol (10 mL) and placed under an argon atmosphere. $Mn(ClO_4)_2$·$6H_2O$ (181 mg, 0.5 mmol) was dissolved in air-free absolute ethanol (10 mL) and placed under an argon atmosphere. This was then added to the previous mixture. A white precipitate appeared rapidly. It was then filtered under an argon atmosphere, and washed with air-free ether (15 mL). A white powder (105 mg, yield = 42%) was then obtained and kept in a glove box until use. Crystallization of complex **1** was performed in the glove box by slow diffusion of diethyl ether in an acetonitrile solution of **1**, and crystals of **1**$(ClO_4)_2$·$2CH_3CN$ suitable for X-ray crystallography study were obtained. It is worth noting that solution and powder samples of **1** are highly sensitive to air oxidation. When not handled under inert atmosphere, complex **1** spontaneously converts into a dark purple species. An X-ray diffraction study revealed that this species is the previously studied mono-μ-oxido dinuclear Mn_2^{III} complex $[(L)Mn(\mu\text{-}O)Mn(L)]^{2+}$ (**3**).[30] **1**$(ClO_4)_2$·$2H_2O$ (powder) ($C_{42}H_{46}Cl_2Mn_2N_8O_{12}$): calcd. C 48.7, H 4.5, Mn 10.6, N 10.8; found C 49.1, H 4.4, Mn 10.3, N 10.6. Note that in the case of the elemental analysis the contamination by species **3** is unapparent. IR: $\tilde{\nu}$ = 3421 (s, strong), 2918 (w, weak), 1634 (s), 1602 (s), 1570 (w), 1552 (w), 1541 (w), 1471 (m, medium), 1442 (m), 1400 (w), 1342 (w), 1295 (m), 1144 (m), 1115 (m), 1089 (s), 1048 (w), 1016 (w), 907 (w), 766 (m), 637 (m), 625 (w), 594 (w) cm^{-1}. ESI-MS: A major peak was detected at m/z = 400 corresponding to $[(L)Mn]^+$.

Infrared Spectroscopy: Spectra were recorded on KBr pellets in the range 4000–400 cm^{-1} with a Perkin–Elmer Spectrum 1000 spectrophotometer.

Electrospray Ionization Mass Spectrometry: Mass spectra were recorded with a Finnigan Mat95 in a BE configuration at low resolution on a micromolar acetonitrile solution.

Elemental Analysis: Analysis was performed by the Service de Microanalyse of the CNRS (Gif-Sur-Yvette, France) for carbon, nitrogen, and hydrogen and by the Service Central d'Analyse (Vernaison, France) for manganese.

X-ray Crystallography: Crystal data for $[(L)MnMn(L)](ClO_4)_2$·$2CH_3CN$ [**1**$(ClO_4)_2$·$2CH_3CN$] and the parameters of data collection are summarized in Table 4. Crystal data for **1**$(ClO_4)_2$·$2CH_3CN$ were collected with a Nonius Kappa-CCD area detector diffractometer using graphite-monochromated Mo-K_α radiation. The lattice parameters were determined from ten images recorded with 2 φ-scans and later refined on all data. The data were recorded at 100°K with an Enraf–Nonius FR558NH nitrogen cryostat. A 180° φ-range was scanned with two steps with a crystal to detector distance fixed at 40 mm. Data was corrected for Lorentz polarization. The structures were solved by the direct methods with SHELXS-97 and refined by full-matrix least-squares on F[2] with anisotropic thermal parameters for all non-H atoms with SHELXL-97. H atoms were found in a difference Fourier map and were introduced at calculated positions as riding atoms, with C–H bond lengths of 0.93 (aromatic CH), 0.98 (aliphatic CH), 0.97 (CH_2), and 0.96 Å (CH_3), and with U_{iso}(H) values of 1.2 U_{eq}(C) for CH and CH_2 hydrogen atoms, and 1.5 U_{eq}(C) for CH_3 hydrogen atoms.

Table 4. Details of structure determination, refinement, and experimental parameters for **1**$(ClO_4)_2$·$2CH_3CN$.

	1$(ClO_4)_2$·$2CH_3CN$
Empirical formula	$C_{46}H_{48}Cl_2Mn_2N_{10}O_{10}$
Formula mass [g mol^{-1}]	1081.72
Temperature [K]	100 (2)
Wavelength [Å]	0.71069
Crystal system	monoclinic
Space group	$P21/n$
a [Å]	8.914(5)
b [Å]	21.075(5)
c [Å]	25.254(5)
α [°]	90.000
β [°]	92.724(5)
γ [°]	90.000
Volume [Å^3]	4739(3)
Z	4
$d_{calcd.}$ [g cm^{-3}]	1.516
Absorption coefficient [mm^{-1}]	0.715
Crystal size [mm]	0.30 × 0.22 × 0.03
Theta range for data collection [°]	2.09 to 30.64
Index ranges	$0 \le h \le 12$
	$0 \le k \le 29$
	$-35 \le l \le 36$
Reflections collected	112633
Independent reflections	13422
	[R(int) = 0.056]
Data [$I > 2\sigma(I)$]	10114
Parameters	655
Goodness-of-fit on F^2	1.049
Final R indices [$I > 2\sigma(I)$]	R_1 = 0.0371
	wR_2 = 0.0963
R indices (all data)	R_1 = 0.0594
	wR_2 = 0.1028
Largest diff. peak/hole [e Å^{-3}]	0.489/–0.497

CCDC-279908 contains the supplementary crystallographic data for this paper. These data can be obtained free of charge from The Cambridge Crystallographic Data Centre via www.ccdc.cam.ac.uk/data_request/cif.

Magnetic Susceptibility Measurements: Magnetic susceptibility data were recorded with an MPMS5 magnetometer (Quantum Design Inc.). The calibration was made at 298 K using a palladium reference sample furnished by Quantum Design Inc. The data were collected over a temperature range of 2–300 K. Above 100 K, a 1 T magnetic field was applied, while below 100 K, the amplitude was 0.1 T. Data were further corrected for diamagnetism. The χ_M vs. T and $\chi_M T$ vs. T curves were fitted by the van Vleck formula assuming the same g factor for each S-spin state. The total spin S runs from $|S_1 - S_2|$ to $(S_1 + S_2)$ by unit steps. The exchange Hamiltonian used was $H = -J\hat{S}_1 \cdot \hat{S}_2$, where J stands for the exchange coupling constant and $\hat{S}_1$, $\hat{S}_2$ for the spin operators associated with the electronic spin of the Mn^{II} sites ($S_1 = S_2 = 5/2$).

EPR Spectroscopy: 9.4 and 34 GHz EPR spectra were recorded with a Bruker ELEXSYS 500 spectrometer. For low temperature studies, an Oxford Instrument continuous-flow liquid helium cryostat and a temperature-control system were used. Solutions spectra

were recorded in acetonitrile containing 0.1 M tetrabutylammonium perchlorate. Quantification of uncoordinated Mn^{II} was performed by comparison of the intensities of the $g = 2$ signal with those obtained using solutions of known concentrations of $Mn(ClO_4)_2 \cdot 6H_2O$ under the same recording conditions. Quantification of complex **4** in situ generated by bulk electrolysis of complex **1** in the presence of base was performed by a comparison of the intensities of the signal with those obtained using solutions of known concentrations of **4** (electrochemically prepared from the one-electron oxidation of **3**, and first isolated as a powder) under the same recording conditions.

UV/Visible Spectroscopy: UV/Visible spectra were recorded with a Varian Cary 300 Bio spectrophotometer at 20 °C with 0.1-cm quartz cuvettes.

Cyclic Voltammetry and Bulk Electrolysis: All electrochemical experiments were run under an Ar atmosphere. Cyclic voltammetry and coulometry measurements were recorded with an EGG PAR potentiostat (M273 model). For the cyclic voltammetry, the counter electrode was a Pt wire and the working electrode a glassy carbon disk carefully polished before each voltammogram with diamond paste (1 μm), sonicated in an ethanol bath and then washed carefully with ethanol. The reference electrode was a $Ag/AgClO_4$ electrode (0.53 V vs. NHE electrode), isolated from the rest of the solution by a fritted bridge. For bulk electrolysis, the counter electrode was a piece of Pt, separated from the rest of the solution with a fritted bridge. The working electrode was a grid of Pt. The solvent used was distilled acetonitrile and tetrabutylammonium perchlorate was added to obtain a 0.1 M supporting electrolyte (20 °C) or a 0.2 M supporting electrolyte (–30 °C). Low temperature regulation was ensured by a Julabo circulation cryostat.

Supporting Information (see also the footnote on the first page of this article): Figure S1: Magnetic susceptibility measurements recorded on complex $\mathbf{1}(ClO_4)_2 \cdot 2H_2O$. Figure S2: EPR spectra of complex $\mathbf{1}(ClO_4)_2 \cdot 2H_2O$ as a function of temperature. Figure S3: EPR spectra of the acetonitrile solution of complex $\mathbf{1}(ClO_4)_2 \cdot 2H_2O$ as a function of temperature. Figure S4: Cyclic voltammograms of the acetonitrile solution of **1** before and after bulk electrolysis at $E = 0.8$ V vs. SCE. Figure S5: UV/Visible spectrum of **4**, electrochemically prepared. Figure S6: 9.4 GHz EPR spectrum of **4**, electrochemically prepared. Figure S7: Evolution of the cyclic voltammograms of the acetonitrile solution of **1** upon addition of chloride ions. Figure S8: Cyclic voltammograms of a 2 mM acetonitrile solution of **5**, after bulk electrolysis at $E = 0.85$ and $E = 1.45$ V vs. SCE. Details of the ^1H NMR spectrum of ligand LH.

Acknowledgments

We are grateful to Félix Perez for mass spectrometry measurements and Dr. Pierre Dorlet for the acquisition of the 34 GHz EPR spectrum. We thank Drs. Elodie Anxolabéhère-Mallart and Geneviève Blondin for stimulating discussions. The Conseil Régional de l'Ile de France is acknowledged for its contribution to the acquisition of the Bruker ELEXSYS X band EPR spectrometer. C. H. acknowledges Dr. Sun Un and Dr. William Rutherford, CEA Saclay, for allowing her to complete the work reported in this paper.

[1] E. J. Larson, V. L. Pecoraro in *Introduction to Manganese Enzymes* (Ed.: V. L. Pecoraro), VCH Publishers, Inc., New York, **1992**, pp. 1–28.
[2] J. D. Crowley, D. A. Traynor, D. C. Weatherburn in *Enzymes and Proteins Containing Manganese: an Overview* (Eds.: A. Sigel, H. Sigel), Marcel Dekker, Basel, Switzerland, **2000**, pp. 209–278.
[3] D. W. Yoder, J. Hwang, J. E. Penner-Hahn in *Metal Ions in Biological Processes* (Eds.: A. Sigel, H. Sigel), Marcel Dekker, New York, **2000**, vol. 37, pp. 527–557.
[4] J. W. Whittaker in *Manganese and Its Role in Biological Processes*, Marcel Dekker, New York, **2000**, vol. 37, pp. 587–611.
[5] A.-F. Miller, *Curr. Opin. Chem. Biology* **2004**, *8*, 162–168.
[6] D. Svedruzic, S. Jonsson, C. G. Toyota, L. A. Reinhardt, S. Ricagno, Y. Lindqvist, N. G. J. Richards, *Arch. Biochem. Biophys.* **2005**, *433*, 176–192.
[7] O. Opaleye, R.-S. Rose, M. M. Whittaker, E.-J. Woo, J. W. Whittaker, R. W. Pickersgill, *J. Biol. Chem.* **2006**, *281*, 6428–6433.
[8] V. J. Just, C. E. M. Stevenson, L. Bowater, A. Tanner, D. M. Lawson, S. Bornemann, *J. Biol. Chem.* **2004**, *279*, 19867–19874.
[9] G. C. Dismukes, *Chem. Rev.* **1996**, *96*, 2909–2926.
[10] N. A. Law, M. T. Caudle, V. L. Pecoraro in *Manganese Redox Enzymes and Model Systems: Properties, Structures, and Reactivity* (Ed.: G. B. Sykes), **1998**, vol. 46, pp. 305–440.
[11] Z. F. Kanyo, L. R. Scolnick, D. E. Ash, D. W. Christianson, *Nature* **1996**, *383*, 554–557.
[12] D. W. Christianson, *Acc. Chem. Res.* **2005**, *38*, 191–201.
[13] W. Oehlmann, U. Griepenburg, G. Auling, *Biotechnol. Lett.* **1998**, *20*, 483–488.
[14] K. N. Ferreira, T. M. Iverson, K. Maghlaoui, J. Barber, S. Iwata, *Science* **2004**, *303*, 1831–1838.
[15] A. W. Rutherford, A. Boussac, *Science* **2004**, *303*, 1782–1784.
[16] S. Mukhopadhyay, S. K. Mandal, S. Bhaduri, W. H. Armstrong, *Chem. Rev.* **2004**, *104*, 3981–4026.
[17] A. J. Wu, J. E. Penner-Hahn, V. L. Pecoraro, *Chem. Rev.* **2004**, *104*, 903–938.
[18] T. G. Carrell, A. M. Tyryshkin, G. C. Dismukes, *J. Biol. Inorg. Chem.* **2002**, *7*, 2–22.
[19] S. Durot, F. Lambert, J.-P. Renault, C. Policar, *Eur. J. Inorg. Chem.* **2005**, *14*, 2789–2793.
[20] S. Durot, C. Policar, F. Cisnetti, F. Lambert, J.-P. Renault, G. Pelosi, G. Blain, H. Korri-Youssoufi, J.-P. Mahy, *Eur. J. Inorg. Chem.* **2005**, *17*, 3513–3523.
[21] M. U. Triller, W.-Y. Hsieh, V. L. Pecoraro, A. Rompel, B. Krebs, *Inorg. Chem.* **2002**, *41*, 5544–5554.
[22] A. Gelasco, V. L. Pecoraro, *J. Am. Chem. Soc.* **1993**, *115*, 7928–7929.
[23] A. K. Poulsen, A. Rompel, C. J. McKenzie, *Angew. Chem. Int. Ed. Engl.* **2005**, *44*, 6916–6920.
[24] L. Sabater, C. Hureau, R. Guillot, A. Aukauloo, *Inorg. Chem.* **2006**, *45*, 2373–2375.
[25] LH: *N*,*N*-bis(2-pyridylmethyl)-*N*′-salicylidenethane-1,2-diamine; mLH: *N*,*N*′-bis(2-pyridylmethyl)-*N*-(2-hydroxybenzyl)-*N*′-methylethane-1,2-diamine; LaH: *N*-(2-hydroxybenzyl)-*N*,*N*′-bis(2-pyridylmethyl)ethane-1,2-diamine; LiH: *N*-(2-hydroxybenzyl)-*N*-(2-pyridylmethyl)-*N*′-(2-pyridyliminato)ethane-1,2-diamine; 2-OHsalpn: 1,3-bis(salicylideneimino)-2-propanol; $L'H_3$: *N*,*N*-bis(2-hydroxybenzyl)-*N*′-2-hydroxybenzylidene-1,2-diaminoethane; H_2BBPEN: *N*,*N*′-bis(2-hydroxybenzyl)-*N*,*N*′-bis(2-methylpyridyl)ethane-1,2-diamine; BPEA: *N*,*N*-bis(2-pyridylmethyl)ethylamine).
[26] C. Hureau, E. Anxolabéhère-Mallart, M. Nierlich, F. Gonnet, E. Rivière, G. Blondin, *Eur. J. Inorg. Chem.* **2002**, 2710–2719.
[27] C. Hureau, L. Sabater, E. Anxolabéhère-Mallart, M. Nierlich, M.-F. Charlot, F. Gonnet, E. Rivière, G. Blondin, *Chem. Eur. J.* **2004**, *10*, 1998–2010.
[28] N. Reddig, D. Pursche, M. Kloskowski, C. Slinn, S. M. Baldeau, A. Rompel, *Eur. J. Inorg. Chem.* **2004**, 879–887.
[29] This notation indicates that there is a mixture in a 1:1 ratio of two complexes in the sample, i.e. $[(Li)MnMn(Li)]^{2+}$ and $[(La)MnMn(Li)]^{2+}$.
[30] O. Horner, E. Anxolabéhère-Mallart, M.-F. Charlot, L. Tchertanov, J. Guilhem, T. A. Mattioli, A. Boussac, J.-J. Girerd, *Inorg. Chem.* **1999**, *38*, 1222–1232.

[31] G. Rogez, A. Marvilliers, P. Sarr, S. Parsons, S. T. Teat, L. Ricard, T. Mallah, *Chem. Commun.* **2002**, 1460–1461.
[32] The *g* value of complex **1** was fixed to 1.95 by analogy to those values of complexes $[(mL)MnMn(mL)]^{2+}$ and $[(Li/La)\text{-}MnMn(Li)]^{2+}$.
[33] Presence of 23% of complex **3** described by $g = 2.0$ and $J = -316\ cm^{-1}$, and of 2.3% of a mononuclear Mn^{II} impurity of half the molar weight of **1** was taken into account.
[34] Presence of 25% of complex **3** described by $g = 2.0$ and $J = -316\ cm^{-1}$, and of 1.5% of a mononuclear Mn^{II} impurity of half the molar weight of **1** was taken into account.
[35] D. P. Kessissoglou, W. M. Butler, V. L. Pecoraro, *Inorg. Chem.* **1987**, *26*, 495–503.
[36] D. Coucouvanis, K. Greiwe, A. Salifoglou, P. Challen, A. Simopoulos, A. Kostikas, *Inorg. Chem.* **1988**, *27*, 593–594.
[37] E. Gallo, E. Solari, N. Re, C. Floriani, A. Chiesi-Villa, C. Rizzoli, *J. Am. Chem. Soc.* **1997**, *119*, 5144–5154.
[38] T. C. Higgs, K. Spartalian, C. J. O'Connor, B. F. Matzanke, C. J. Carrano, *Inorg. Chem.* **1998**, *37*, 2263–2272.
[39] H. Adams, N. A. Bailey, N. Debaeker, D. E. Fenton, W. Kanda, J.-M. Latour, H. Okawa, H. Sakiyama, *Angew. Chem. Int. Ed. Engl.* **1995**, *34*, 2535–2537.
[40] B. Albela, M. Corbella, J. Ribas, I. Castro, J. Sletten, H. Stoeckli-Evans, *Inorg. Chem.* **1998**, *37*, 788–798.
[41] T. Howard, J. Telser, V. J. DeRose, *Inorg. Chem.* **2000**, *39*, 3379–3385.
[42] I. Romero, M.-N. Collomb, A. Deronzier, A. Llobet, E. Perret, J. Pécaut, L. Le Pape, J.-M. Latour, *Eur. J. Inorg. Chem.* **2001**, 69–72.
[43] E. J. Laskowski, D. N. Hendrickson, *Inorg. Chem.* **1978**, *17*, 457–470.
[44] H. Schmitt, R. Lomoth, A. Magnuson, J. Park, J. Fryxelius, M. Kritikos, J. Martensson, L. Hammarström, L. Sun, B. Akermark, *Chem. Eur. J.* **2002**, *8*, 3757–3767.
[45] $E^{1/2}$ is defined as $1/2\cdot(E^{Pa} + E^{Pc})$ and $\Delta E^{P} = |E^{Pa} - E^{Pc}|$ where E^{Pa} (E^{Pc}) is defined as the potential of the maximum of current intensity when scanning toward anodic (cathodic) potentials.
[46] J. B. Vincent, K. Folting, J. C. Huffman, G. Christou, *Inorg. Chem.* **1986**, *25*, 996–999.
[47] M. Suzuki, M. Mikuriya, S. Murata, A. Uehara, H. Oshio, S. Kida, K. Saito, *Bull. Chem. Soc. Jpn.* **1987**, *60*, 4305–4312.
[48] H. Diril, H.-R. Chang, M. J. Nigles, X. Zhang, J. A. Potenza, H. J. Schugar, S. S. Isied, D. N. Hendrickson, *J. Am. Chem. Soc.* **1989**, *111*, 5102–5114.
[49] R. Lomoth, P. Huang, J. Zheng, L. Sun, L. Hammarström, B. Akermark, S. Styring, *Eur. J. Inorg. Chem.* **2002**, 2965–2974.
[50] A. Gelasco, M. L. Kirk, J. W. Kampf, V. L. Pecoraro, *Inorg. Chem.* **1997**, *36*, 1829–1837.
[51] C. Hureau, S. Blanchard, M. Nierlich, G. Blain, E. Rivière, J.-J. Girerd, E. Anxolabéhère-Mallart, G. Blondin, *Inorg. Chem.* **2004**, *43*, 4415–4426.
[52] C. Hureau, G. Blondin, M.-F. Charlot, C. Philouze, M. Nierlich, M. Césario, E. Anxolabéhère-Mallart, *Inorg. Chem.* **2005**, *44*, 3669–3683.
[53] The intensity of the cathodic process detected at $E^{P} = -0.52$ V vs. SCE is unchanged upon the addition of the base, confirming that the complex **3** is formed at the electrode and not directly in solution.
[54] A. Neves, S. M. D. Erthal, I. Vencato, A. S. Ceccato, Y. P. Mascarenhas, O. R. Nascimento, M. Hörner, A. A. Batista, *Inorg. Chem.* **1992**, *31*, 4749–4755.
[55] A. Abragam, B. Bleaney, *Electron Paramagnetic Resonance of Transition Ions*, Dover Publications, Inc., New York, **1970**.
[56] F. E. Mabbs, D. Collison, *Electron Paramagnetic Resonance of d Transition Metal Compounds*, Elsevier Science Publishers B. V., Amsterdam, The Netherlands, **1992**, vol. 16.
[57] C. J. H. Jacobsen, E. Pedersen, J. Villadsen, H. Weihe, *Inorg. Chem.* **1993**, *32*, 1216–1221.
[58] D. De Vos, B. M. Weckhuysen, T. Bein, *J. Am. Chem. Soc.* **1996**, *118*, 9615–9622.
[59] L. S. Erre, G. Micera, E. Garribba, A. C. Bényei, *New J. Chem.* **2000**, *24*, 725–728.
[60] It is not rigorously correct to note complex **5** as a mixture of complex **1** and chloride ions in a 1:2 ratio based on the presence of an equilibrium between these three species. However, we will do it for clarity.
[61] M. P. Hendrich, P. G. Debrunner, *Biophys. J.* **1989**, *56*, 489–506.
[62] J. Krzystek, J. Telser, *J. Magn. Reson.* **2003**, *162*, 454–465.
[63] H. J. Gerritsen, E. S. Sabisky, *Phys. Rev.* **1963**, *132*, 1507–1512.
[64] S. L. Dexheimer, J. W. Gohdes, C.-W. Chan, K. S. Hagen, W. H. Armstrong, M. P. Klein, *J. Am. Chem. Soc.* **1989**, *111*, 8923–8925.
[65] K. A. Campbell, E. Yikilmaz, C. V. Grant, W. Gregor, A.-F. Miller, R. D. Britt, *J. Am. Chem. Soc.* **1999**, *121*, 4714–4715.
[66] S. R. Morrissey, T. E. Horton, C. V. Grant, C. G. Hoogstraten, R. D. Britt, V. J. DeRose, *J. Am. Chem. Soc.* **1999**, *121*, 9215–9218.
[67] K. A. Campbell, D. A. Force, P. J. Nixon, F. Dole, B. A. Diner, R. D. Britt, *J. Am. Chem. Soc.* **2000**, *122*, 3754–3761.
[68] K. A. Campbell, M. R. Lashley, J. K. Wyatt, M. H. Nantz, R. D. Britt, *J. Am. Chem. Soc.* **2001**, *123*, 5710–5719.
[69] M. Maneiro, M. R. Bermejo, M. Fondo, A. M. González, J. Sanmartin, J.-C. Garcia-Monteagudo, R. G. Pritchard, A. M. Tyryshkin, *Polyhedron* **2001**, *20*, 711–719.
[70] As pointed out by one of the referees, the one-electron oxidation of species **6** may also lead to the formation of the Mn^{III}-phenoxyl species. For the reason given in the text and from the data previously reported in the literature concerning related complexes (see ref. [54,71,75–78]), we strongly favor the formation of a Mn^{IV}-phenolate as the predominant species. Therefore, for the sake of clarity, we describe species **7** as the Mn^{IV}-phenolate species. However, we acknowledge that we have no conclusive argument to definitively rule out the presence in solution of the Mn^{III}-phenoxyl as a minor species. More generally, the correct description of the one-electron oxidation product of the Mn^{III}-phenolate species is still an open debate. As suggested by the referee, XAS studies would help to disentangle this issue and should be the subject of future reports.
[71] B. Adam, E. Bill, E. Bothe, B. Goerdt, G. Haselhorst, K. Hildenbrand, A. Sokolowski, S. Steenken, T. Weyhermüller, K. Wieghardt, *Chem. Eur. J.* **1997**, *3*, 308–319.
[72] Note that the molar extinction coefficient values have been estimated assuming the formation of 95% of the Mn^{IV} species.
[73] C. Hureau, Thèse de l'Université Paris-Sud, Orsay, **2003**.
[74] D. R. Gamelin, M. L. Kirk, T. L. Stemmler, S. Pal, W. H. Armstrong, J. E. Penner-Hahn, E. I. Solomon, *J. Am. Chem. Soc.* **1994**, *116*, 2392–2399.
[75] U. Auerbach, T. Weyhermüller, K. Wieghardt, B. Nuber, E. Bill, C. Butzlaff, A. X. Trautwein, *Inorg. Chem.* **1993**, *32*, 508–519.
[76] M. J. Baldwin, T. L. Stemmler, P. J. Riggs-Gelasco, M. L. Kirk, J. E. Penner-Hahn, V. L. Pecoraro, *J. Am. Chem. Soc.* **1994**, *116*, 11349–11356.
[77] C. Hureau, E. Anxolabéhère-Mallart, G. Blondin, E. Rivière, M. Nierlich, *Eur. J. Inorg. Chem.* **2005**, *23*, 4808–4817.
[78] N. A. Law, T. E. Machonkin, J. P. McGornam, E. J. Larson, J. W. Kampf, V. L. Pecoraro, *J. Chem. Soc., Chem. Commun.* **1995**, *19*, 2015–2016.
[79] C. Hureau, L. Sabater, F. Gonnet, G. Blain, J. Sainton, E. Anxolabéhère-Mallart, *Inorg. Chim. Acta* **2006**, *359*, 339–345.
[80] D. T. Richens, D. T. Sawyer, *J. Am. Chem. Soc.* **1979**, *101*, 3681–3683.
[81] D. P. Kessissoglou, X. Li, W. M. Butler, V. L. Pecoraro, *Inorg. Chem.* **1987**, *26*, 2487–2492.
[82] S. K. Chandra, P. Basu, D. Ray, S. Pal, A. Chakravorty, *Inorg. Chem.* **1990**, *29*, 2423–2428.
[83] S. M. Saadeh, M. S. Lah, V. L. Pecoraro, *Inorg. Chem.* **1991**, *30*, 8–15.

[84] O. Schlager, K. Wieghardt, B. Nuber, *Inorg. Chem.* **1995**, *34*, 6456–6462.
[85] T. M. Rajendiran, J. W. Kampf, V. L. Pecoraro, *Inorg. Chim. Acta* **2002**, *339*, 497–502.
[86] T. K. Paine, T. Weyhermüller, E. Bothe, K. Wieghardt, P. Chaudhuri, *Dalton Trans.* **2003**, *15*, 3136–3144.
[87] B. H. Huynh, T. A. Kent in *Advances in Mössbauer Spectroscopy* (Eds.: B. V. Thosar, P. K. Iyengar, J. K. Srivastava, S. C. Bhargava), Elsevier, New York, **1983**, p. 490.
[88] P. Hapiot, L. D. Kispert, V. V. Konovalov, J.-M. Savéant, *J. Am. Chem. Soc.* **2001**, *123*, 6669–6677.
[89] O. Horner, M.-F. Charlot, A. Boussac, E. Anxolabéhère-Mallart, L. Tchertanov, J. Guilhem, J.-J. Girerd, *Eur. J. Inorg. Chem.* **1998**, 721–727.

Received: March 28, 2006
Published Online: September 13, 2006

